Challenge Track project: Experimental subatomic physics

Esben R. Christensen (201406233)

June 9, 2017

Abstract

Based on data from the ISOLDE-experiment IS605 (undertaken May 2016), this project investigates angular distributions and correlations of particles involved in the β-delayed α-decay of ^{16}N. The experiment utilized five DSSDs backed by four PADs. Distributions of the relative angles of α-^{12}C-particles are found from DSSD-detections and compared to a Monte Carlo simulation of the reaction. The simulated angular distribution shows great dependence on beam width and position. Good discrepancy is found if the right beam position is chosen. The simulation shows that the spatial resolution of the DSSDs is not high enough to show much dependence on whether a recoil of ^{16}O is accounted for or not. Angular correlations between α- and β-particles is studied by utilizing data in the PADs. PADs P6 and P4 are not used because of technical disturbance in their spectra. Two approaches to correct for trigger cutoffs are used. A χ^2-independence test for angular correlation yields p-values of 0.035 and 0.044 for approach 1 and 2, respectively. The p-values are estimated to be higher than this because of negligence of uncertainties in the expected values. Approach 2 is believed to be most correct and with added uncertainties it should show very little or no correlation between α- and β-particles. Given the lack of sensitivity towards recoil of ^{16}O, the interesting angular correlation between $\bar{\nu}_e$ and β will be difficult to investigate with the given data.

1 Introduction

This is a project report of the Challenge Track project *Experimental subatomic physics* under the supervision of Oliver Kirsebom (main supervisor) and Hans Fynbo. The project takes its starting point in the data collected in the ISOLDE-experiment IS605 performed in May 2016 by Oliver Kirsebom among others. The main focus has been to investigate angular distributions and correlations between particles involved in the β-delayed α-decay of ^{16}N.

Put very briefly, in the experiment, a beam of ^{16}N particles is sent from an accelerator into a thin slice of silicon where it stops and decays to $^{16}\text{O}^* + e^- + \bar{\nu}_e$, i.e. β^--decay. The excited oxygen then decays to $^{12}\text{C} + \alpha$. The information from the angular correlation of $\bar{\nu}$ and e^- could give information of the original state of ^{16}N (Hong, Sternberg, and Garcia 2017, p. 6). This correlation is difficult to find since it demands very low energy thresholds and a high spatial resolution of the detectors. Only the first steps in such an analysis are taken in this report. Of interest is the distribution of the relative angles of α-^{12}C-coincidences along with angular correlations of α-β-coincidences. Since the β-particles are detected in the detectors with no spatial resolution (PADs), the relative angle between an α- and β-particle cannot be calculated directly. The data does allow for a rough analysis of any angular correlation between these two particles, and this is carried out.

In the report, preliminary results and other findings are also shown in order to give a characterization of the data set. This information can also be used for later work with the data set. The project is pure analysis of data, but most necessary details about the experiment are given below.

2 Experimental set up

In this section a brief description of the ISOLDE-experiment IS605 is given. Only the most relevant information for this project is given, for more details of the actual goal of the experiment see reference (Fynbo, Kirseboom, and Tengblad 2017).

As mentioned, in the ISOLDE-experiment IS605, a beam of ^{16}N particles is sent from an accelerator into a thin slice of silicon where it stops and decays to $^{16}\text{O}^* + e + \bar{\nu}_e$. The excited oxygen then decays to $^{12}\text{C} + \alpha$. The experiment utilizes DSSD detectors, i.e. double-sided silicon strip detectors, to detect α-particles that have energies roughly between 1 and 2.5 MeV. Four DSSDs are placed around the target and one beneath it, see Figure 1. The four DSSDs surrounding the target are backed by unsegmented

silicon-pad detectors, PADs. The DSSDs and PADs are all 50 mm by 50 mm but vary in thicknesses. In Table 1 are given the DSSDs and associated PADs (the PADs behind them) with *id* and thickness. All DSSDs, except the bottom one, U5, are backed by PADs that are numbered according to which DSSD they are behind. E.g. U1 is backed by the PAD P1. The number *id* is the detector identification in the data treatment program ROOT which has been used to analyze the data. It will not be important for the report that ROOT has been used, but some of the information, like *id*, and generating commands have been left on the plots for the initiated reader. Also, some terminology that will be used often like "multiplicity" stems from the data structure in ROOT, and should be briefly elaborated on: In ROOT, the data is accessed from a tree that consists of different branches. The most important branches for the analysis have been *mul*, specifying how many particles have been detected in each event (decay), *FE*, an array of length *mul* specifying the detected energy of each of the detected particles, and also a few other branches specifying the positions of the detected particles. With the most necessary information about the experiment at hand, it is possible to present the findings of the project.

DSSD and PAD information

DSSD (id)	U1 (0)	U3 (1)	U4 (2)	U5 (3)	U6 (4)
Thickness (μm)	42	60	300	1000	60
Associated PAD	P1 (5)	P3 (6)	P4 (7)	NA	P6 (8)
Thickness (μm)	1000	1000	500	NA	500

Table 1: The thickness and id of each DSSD and associated PADs is given. The information can also be seen in Figure 1.

Experimental Set-up

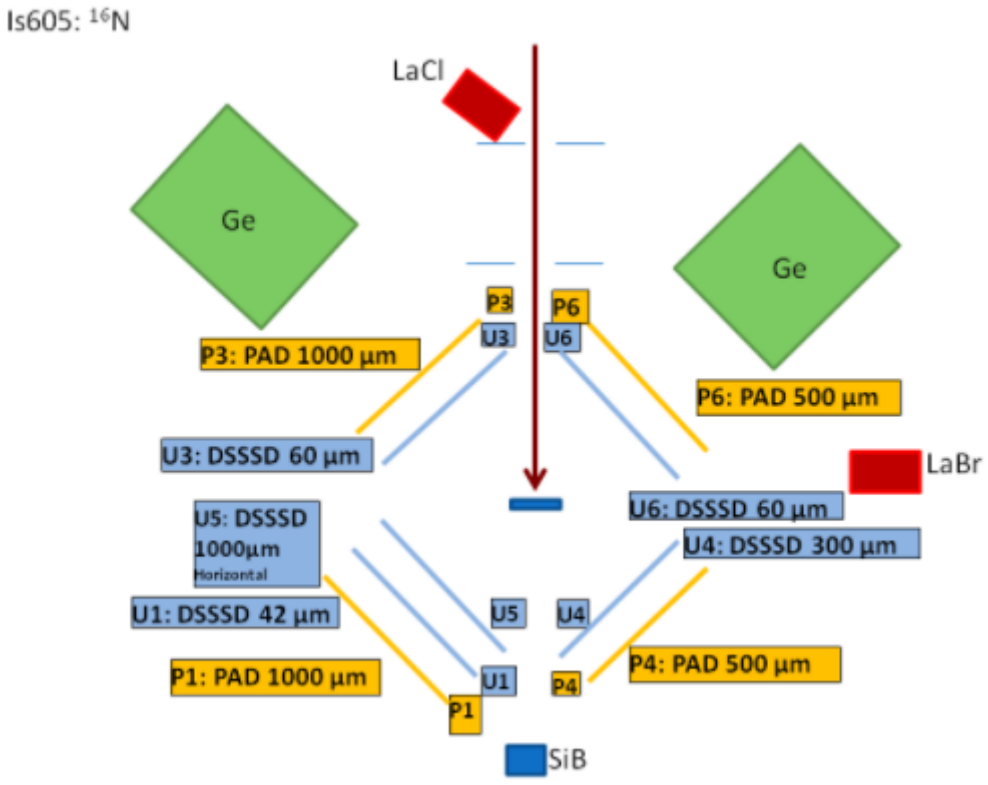

Figure 1: Experimental Set-up of IS605. A silicon target is surrounded by four DSSDs backed by four PADs. Underneath the target is also a DSSD (U5). Figure is taken from the ELOG summary report of the experiment made by Oliver Kirsebom, 2016.

3 Preliminary investigations

In this section, preliminary investigations of the experimental data are presented. The findings in this section serve more as a documentation and motivation of the methods used in the next sections.

As seen in Table 1, detectors U6 and U5 are examples of thin and thick detectors respectively. Each detector has advantages and disadvantages depending on what is to be analyzed. Only the thin detectors are able to separate α-spectrum from the β-background. This can be seen in the energy spectrum plots for detectors U6 and U5, in Figure 2 and Figure 3 respectively.

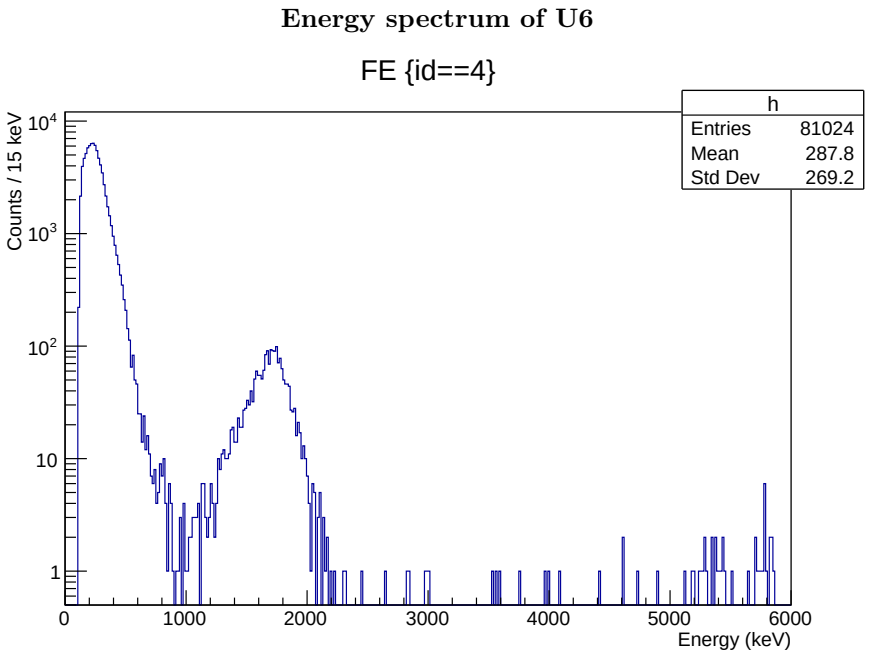

Figure 2: An example of an energy spectrum. This is for detector U6, log scale. α-particles are discernable between 1 and 2.5 MeV. Also low-energy ^{12}C and β-particles are detected.

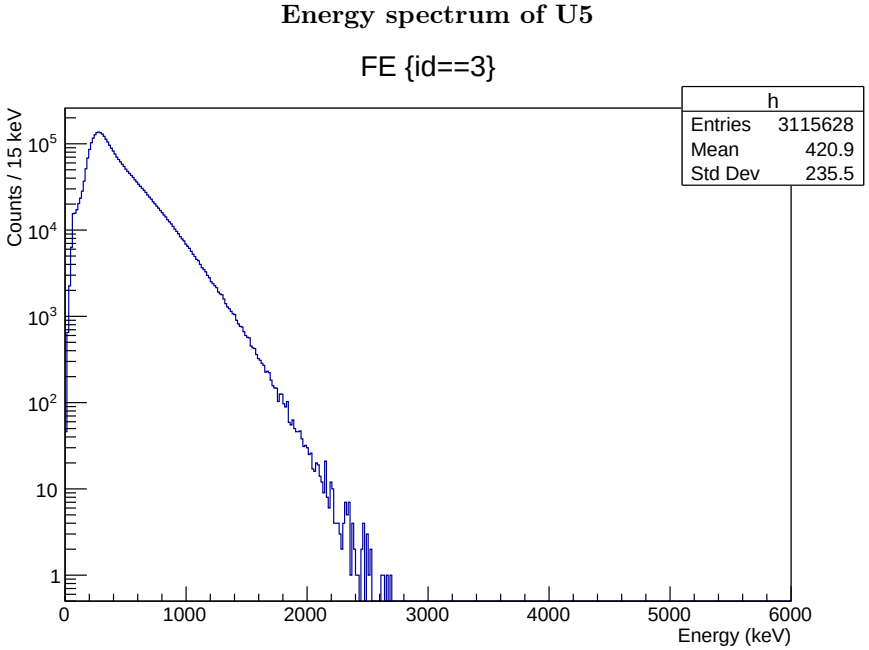

Figure 3: An example of an energy spectrum. This time for detector U5, log scale. The α-particles drown in the β-background.

From Figure 2 and Figure 3, it is seen that there are great differences between the detector spectra, which is due to the width of the active areas inside them. In terms of detecting α- and ^{12}C-particles, the

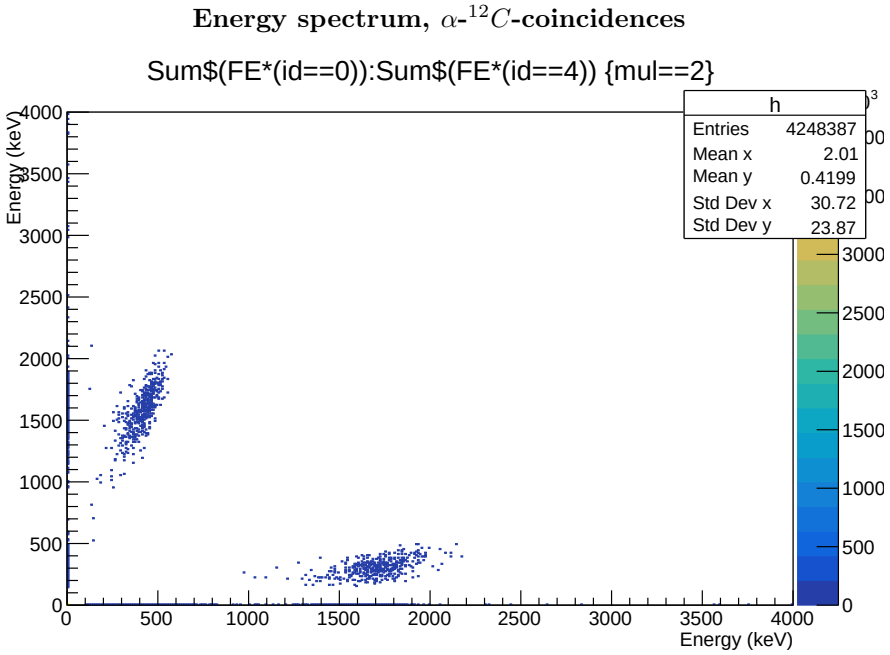

Figure 4: An energy against energy plot for two-particle events. One particle is detected in U1 and one in U6, these face opposite each other and it is seen that the bands follow α-^{12}C-energy distributions, i.e. straight lines with slopes that are the ratios of the masses.

focus will have to be on the three thin detectors U1, U3 and U6. For these detectors it is of interest to look at the available statistics and verify which conditions yield α-^{12}C-coincidences.

It is expected that an α- and ^{12}C-particle will be sent out back to back, i.e. at a relative angle of approximately 180 degrees. This means that if the multiplicity of an event is set to be 2, and the data is restricted to detectors that are facing opposite to each other, α and ^{12}C pairs are expected. Energy-wise it can be shown from momentum conservation that

$$T_C = \frac{m_\alpha}{m_C} T_\alpha, \tag{1}$$

where T and m are the kinetic energy and mass, and the subscripts indicate the associated particle. The ratio m_C/m_α is approximately 3. The formula in Equation 1 is under the assumption that the parent nucleus is at rest before and after the reaction so the formula should only be taken as an approximation. It predicts that if the energies of the α-particles are plotted against the energies of their ^{12}C-partners they should follow a straight line. This is seen in Figure 4. Roughly speaking, the bands follow lines with slopes that correspond to the mass ratios of either 3 or 1/3. The band with slope 1/3 corresponds to an α in detector U6 and a ^{12}C in U1 and vice versa for the band with slope 3. Having identified α- and ^{12}C-pairs, the relative angles between the particles are to be extracted.

4 Angular distribution between α-^{12}C

Using a Monte Carlo simulation routine, provided by the group, it has been possible to simulate α-and ^{12}C-products from the reaction $^{16}O^* \longrightarrow \alpha +^{12} C$, where $^{16}O*$ was in turn a decay product from ^{16}N. To find the angular distribution of the experimental data, a C++-macro is made that extracts the position vectors of the α- and ^{12}C-pairs. The relative angle is then found as

$$\theta = \arccos\left(\frac{\vec{r}_\alpha \cdot \vec{r}_C}{\|\vec{r}_\alpha\|\|\vec{r}_C\|}\right), \tag{2}$$

where $\vec{r}_\alpha$ and $\vec{r}_C$ are the position vectors of the α- and ^{12}C-particle, respectively. The first simulation result is shown in Figure 5. Here the reaction is normal in the sense that a small recoil of the parent nucleus ^{16}O is taken into account, which should reduce the relative angle between α- and ^{12}C-products slightly. The particle beam of ^{16}N is also taken to have a finite width of 3 mm. It is set to hit the point $(1.5, 0, -2.7)$, which is believed to be close to the actual experiment beam position. The simulated data in Figure 5, red, is seen to differ a little from the experimental data in that it is a little shorter. Note

that in the simulation it is exploited that a lot more data can be generated. This means that the number of events is $N = 10^6$, while it was only around 2000 in the experiment. The histograms have been scaled with respect to each other so that they can be compared. It is interesting to see whether the recoil of

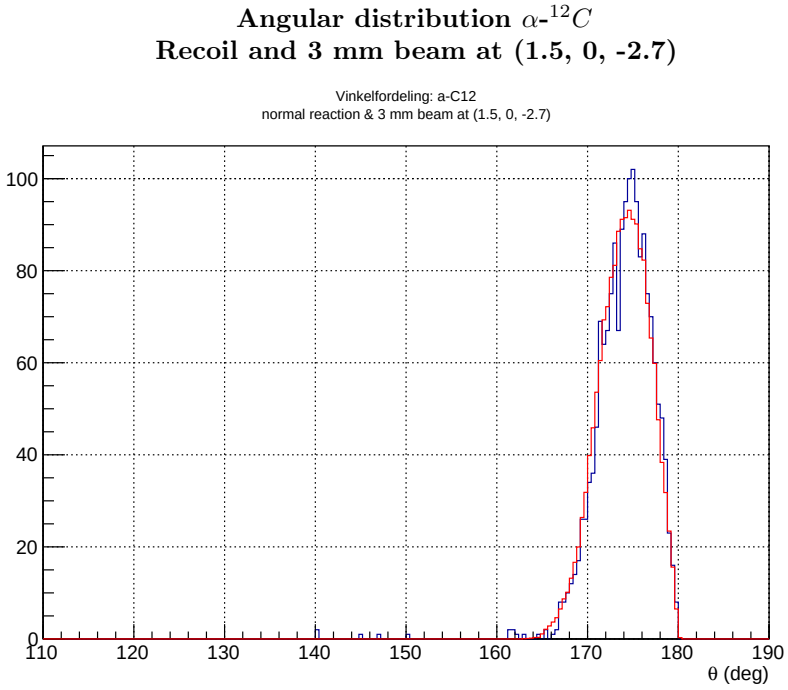

Figure 5: Comparison of simulated (red) and experimental data (blue) of angular distribution of α in detector U1 and ^{12}C in detector U6 *with* recoil and a beam with finite width (3 mm). Beam is centered at (1.5,0,-2.7). Conditions are one α and one ^{12}C in each detector.

$^{16}O*$ or the beam radius and position affects the angular distribution the most. In Figure 6, the position of the beam and target have been changed to the origin $(0, 0, 0)$, while the reaction is normal and beam width is still 3 mm. It is seen that the angles are now generally higher than what the experiment showed. The distribution also seem to be narrower.

In Figure 7, the reaction is still normal with recoil included but the beam is now a point beam, hitting the origin. It is seen that this also affects the simulated data further. The distribution is now much closer to 180 degrees and narrower.

The last case examined is where the recoil is dropped and the parent nucleus is assumed to be at rest before and after the reaction, while the beam has once again a finite width of 3 mm. The results are seen in Figure 8, and it is seen that the simulated data is much like the case where the reaction included a recoil and still a finite beam width, see Figure 6.

Three cases have been presented, and the radius and position of the beam have much more to say than if the reaction has recoil or not. I.e. the uncertainty in the beam and its position means that the detectors are not sensitive to the recoil. A sufficiently small pixel size of the detectors would reveal an effect of a missing recoil. Also, the beam position of (1.5, 0, -2.7) seems to be close to the actual experimental position and the small deviations in height of the distributions in Figure 5 can probably be made less by tweaking the beam position.

Angular distribution α-^{12}C
Recoil and 3 mm beam at origin

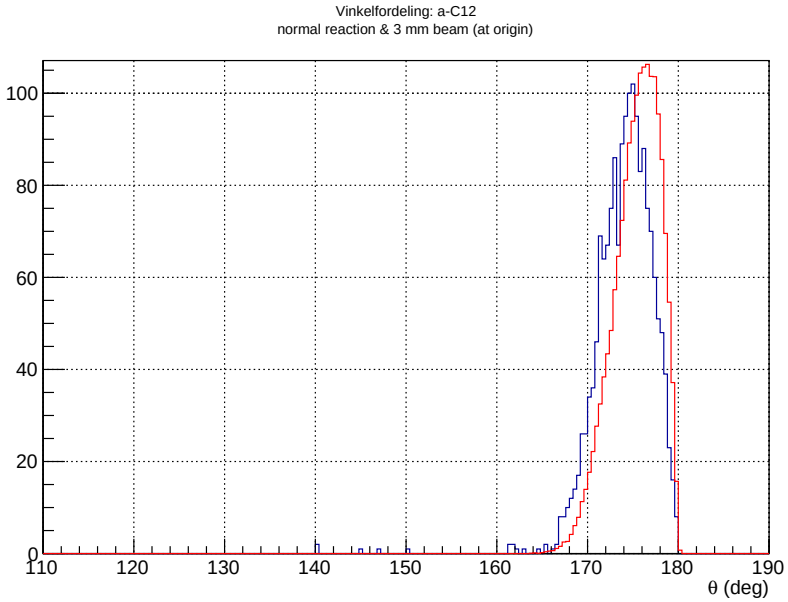

Figure 6: Comparison of simulated (red) and experimental data (blue) of angular distribution of α in detector U1 and ^{12}C in detector U6 with recoil and a beam with finite width. The beam and target positions are now in the origin (0,0,0).

Angular distribution α-^{12}C
Recoil and point beam at origin

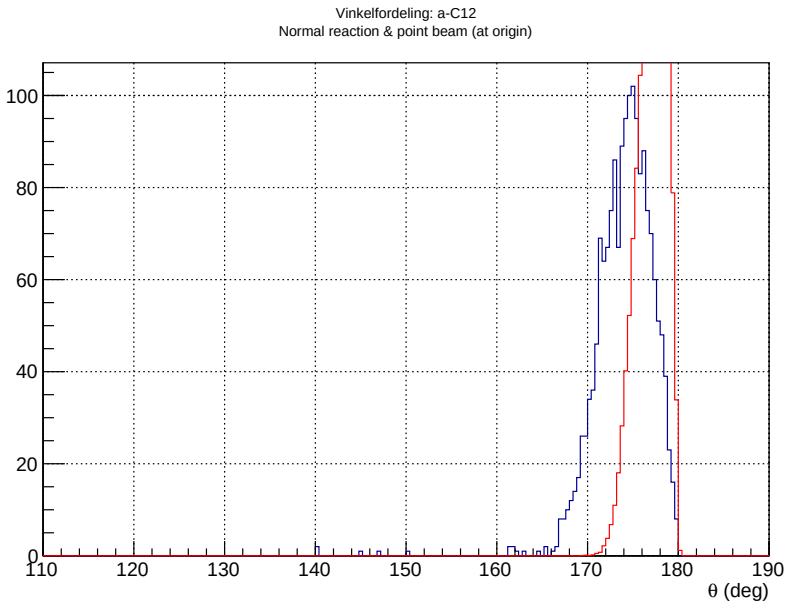

Figure 7: Comparison of simulated (red) and experimental data (blue) of angular distribution α U1 and ^{12}C in detector U6 with recoil accounted for, but point beam with position in origin.

Angular distribution α-^{12}C
No recoil and 3 mm beam at origin

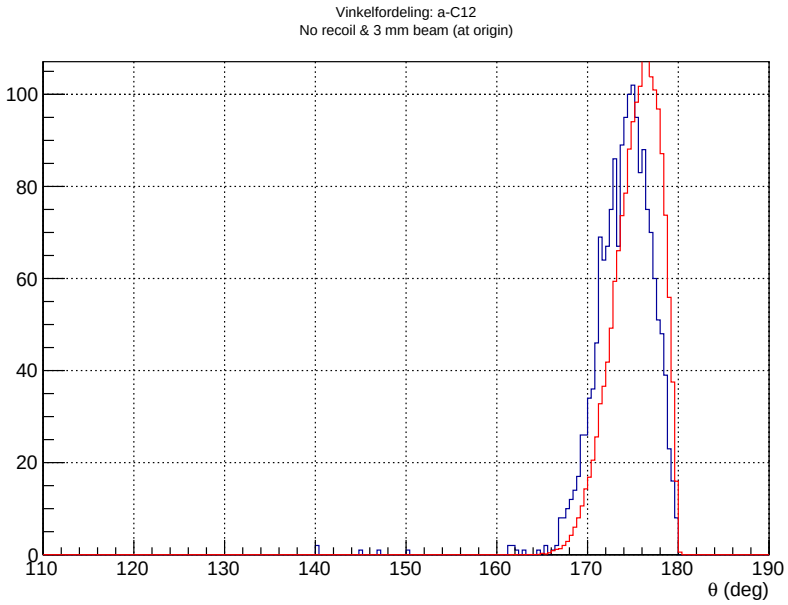

Figure 8: Comparison of simulated (red) and experimental data (blue) of angular distribution of α in detector U1 and ^{12}C in detector U6. Finite beam width of 3 mm in origin, but no recoil in the reaction.

5 Preliminary investigations: α-β-coincidences

It is now time to investigate the angular correlation between α- and β-particles, and first step is to get an idea of the statistics at hand. The PADs are now exploited since they have low energy thresholds and an appropriate depth for detection of β-particles. It is quite certain that α- and ^{12}C-particles are stopped in the DSSDs, so that a signal in a PAD can to a good approximation be taken as being a β-particle (at least for some of the PADs, as is shown below).

Given *one* α in detector U1, say, an associated signal in one of the PADs might be detected. Remember that an α-detection is taken to be a signal in a DSSD that has energy between 1 and 2.5 MeV which has been shown to be a good approximation in the preliminary analysis. The data under these conditions is seen in Table 2. In some events, where an α is given, there will be no signal in any of the PADs at all. If one takes into account the thicknesses of the PADs, it is seen that P6 has more counts than expected. P1 and P3 are comparable in thickness and distance from target and seem to show similar counts. Something strange is clearly going on with P6. In the Appendix is also provided a Table showing the β-statistics for the events with α-^{12}C-coincidences, and it should be noted that this data also shows the same tendency just with less statistics, i.e. P6 is over represented.

β-distributions, given α

DSSD (id)	$\#\alpha$	$\#\beta$, %	P1 %	P3 %	P4 %	P6 %	U5 %
U1 (0)	2536	1555, 61.3	11.4	10.9	4.4	61.0	12.3
U3 (1)	1960	1232, 62.9	12.3	9.7	6.5	58.3	13.1
U6 (4)	1995	1287, 64.5	11.5	10.5	5.1	57.3	15.5

Table 2: Table showing the number and distribution of β-particles given one α in either U1, U3 or U6. The column $\#\alpha$ gives the number of α's detected in the given detector. For each α-detection there can be a β-detection, and the column $\#\beta$ gives the number of times a β-particle was also detected. For each pad there is a column specifying the percentages of β's that were detected here. E.g., 2536 α-particles were recorded in U1, 61.3 % of these, 1555, had an associated β-detection in a pad, and 11.4 % of these were detected in P1.

The spectrum of P6 (and also of P4) is shown to try to gain insight into what is going. The real conclusion is that the PADs P6 and P4 have in some technical way been influenced by the γ-detectors of the experiment. This information has been provided by the group. In Figure 9 and Figure 10 the energies of the signals detected in P6, under the given condition, are shown in normal and log-scale, respectively. It is seen in Figure 10 that there are many counts of very low energy, and then a more rounded distribution around 200 keV riding on top of these counts. This could be the β-particles.

The β energy spectrum of the PAD P4 is also shown, Figure 11. The behavior is reminiscent of that in Figure 9 only that the number of counts is much lower and a higher threshold seems to have been triggered than for P6. As will be shown in the next section, the spectra for P6 and P4 differ greatly from those for P1, P3, and U5 which look more like rounded like classic β-energy spectra. P6 and P4 will therefore not be used in the subsequent analyses.

Energy spectrum of P6, given an α

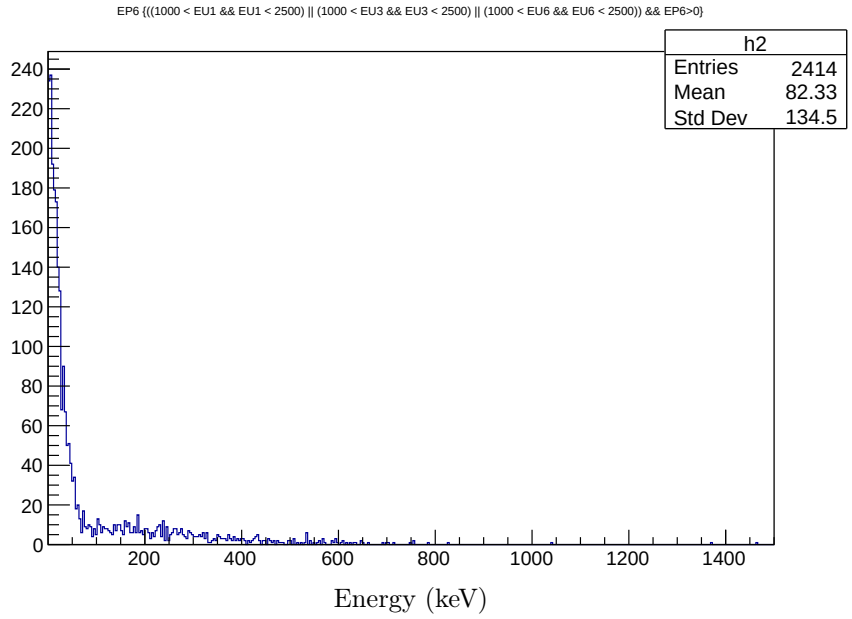

Figure 9: The β energy spectrum of P6, the requirement being that an α-particle is detected in either U1, U3 or U6. A lot of low-energy counts appear and a more rounded distribution rides on top of this.

Energy spectrum of P6 (log-scale), given an α

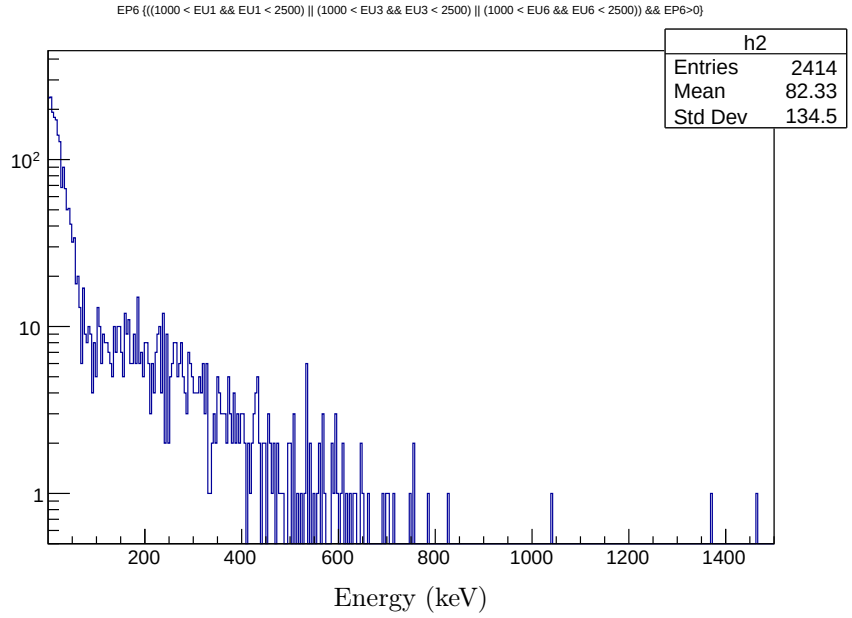

Figure 10: The same β energy spectrum of P6 as in Figure 9. The low-energy counts are an order of magnitude more abundant than the rounded distribution that rides on top of them, which is seen more clearly in this plot as opposed to the absolute scale plot.

Energy spectrum of P4, given an α

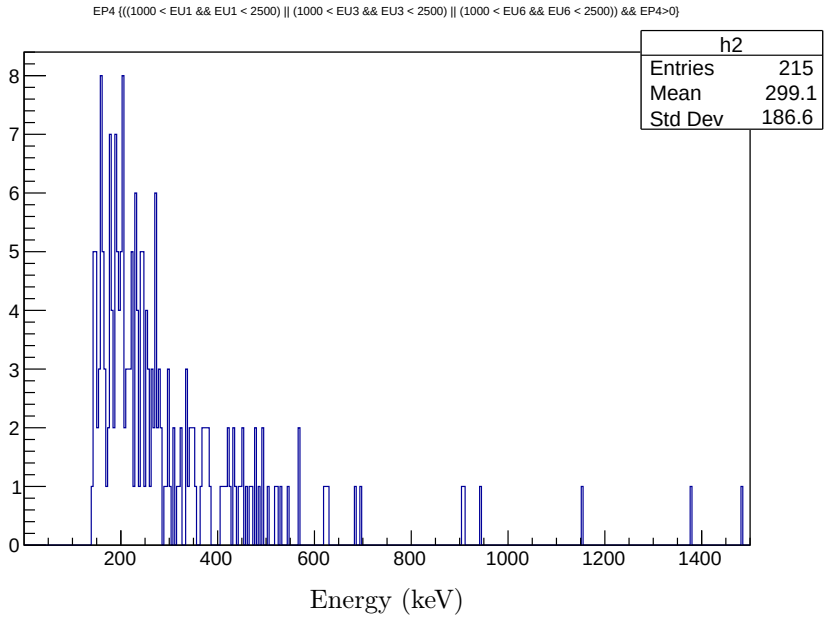

Figure 11: The energy spectrum detected in P4. Only requirement is that an α-particle is detected in either U1, U3 or U6. Some noise seems to present.

β-spectra of P1, P3, and U5

The analysis of angular correlation is continued by studying the spectra from P1, P3 and also U5, the latter being thick enough to detect β-particles like the PADs. In Figure 12, Figure 13 and Figure 14 the β energy spectra are seen for P1, P3, and U5 are seen. Again, the condition is that an α is detected in either U1, U3, or U6. The spectra in Figure 12 and Figure 13 are similar. From around 200 keV and up, the spectra seem to be distributed like a parabola, but from about 200 and down the spectra do not fall off as one might expect. Rather, they seem to increase again. The spectrum in Figure 14 from U5 shows less signs of disturbance in the low energies and falls off a more steadily towards zero. The differences in how the spectra behave in the low energy regime and differences in the detector cutoff motivates an attempt to estimate the cutoff counts. Before this is done, the number of β-particles in P1, P3, and U5 are shown in Table 3 for the three cases an α-particle in either U1, U3, or U6. At this point it is not possible to say much about the correlation (or lack thereof) since no cutoffs and expected values have been calculated. This is treated in the next section.

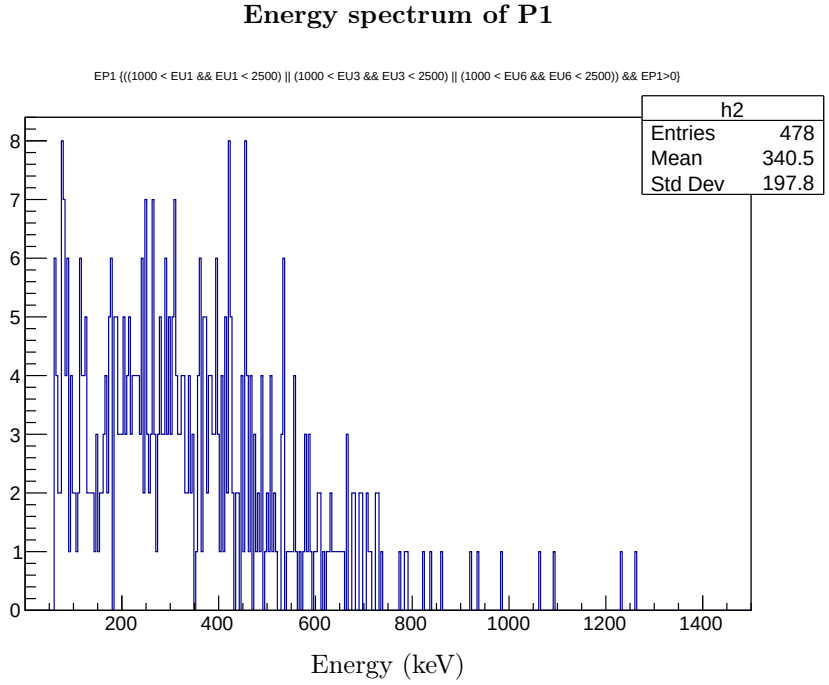

Figure 12: The detection spectrum in P1 with the only requirement that an α-particle is detected in either U1, U3 or U6. Some unexpected behavior is seen for low energies.

Energy spectrum of P3

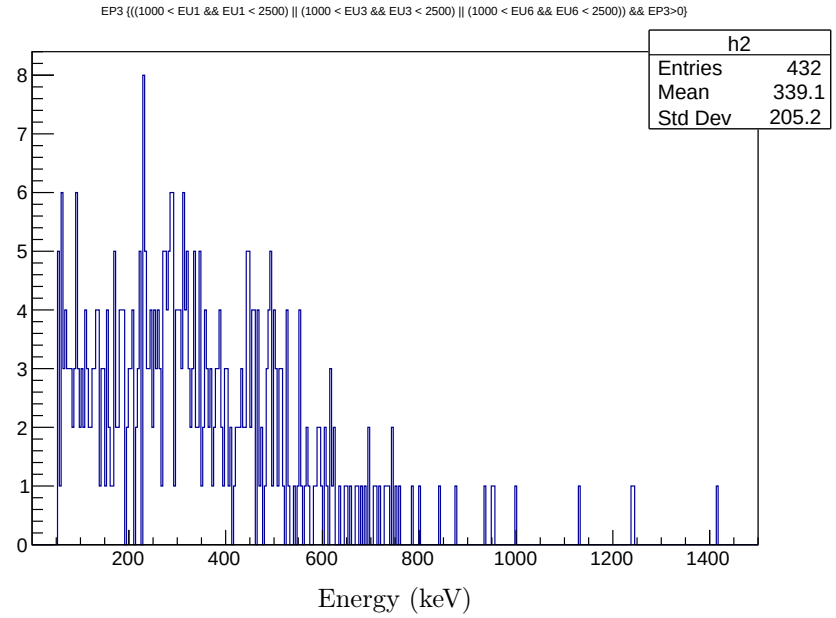

Figure 13: The detection spectrum in P3 with the only requirement that an α-particle is detected in either U1, U3 or U6. Some disturbance is seen for low energies.

Energy spectrum of U5

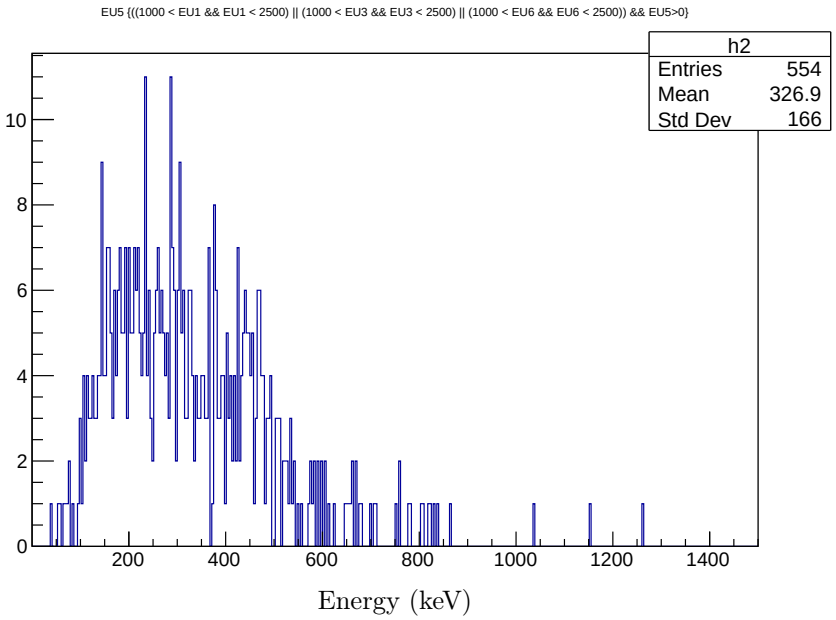

Figure 14: The detection spectrum in U5 with the only requirement that an α-particle is detected in either U1, U3 or U6. The spectrum falls off to zero for low energies.

Distribution of β-particles, raw data

α in DSSD (id)	β in P1	β in P3	β in U5
U1 (0)	177	170	191
U3 (1)	152	120	162
U6 (4)	148	135	200

Table 3: The table shows the detected β-particles given an α in one of the DSSDs U1, U3, or U6. The data is raw in the sense that no cutoffs have been added.

6 Angular correlation of α-β

In this section the angular correlation between α- and β-particles is estimated. Since the PADs have no spatial resolution other than the 50 mm by 50 mm area that they occupy, the correlation sought for is large scale. In the β spectra shown there seemed to be both disturbances at low energies combined with different trigger cutoffs. These effects should be compensated for before any correlation can be estimated. Also, the expected counts for each detector should be calculated which is the first task.

Expected counts

Ideally, the situation is the following (P1 as example):

$$N^{P1}_{\beta,tot} = N^{P1}_{\beta,detected} + \text{corr.}^{P1}, \tag{3}$$

which says that the total number of β-particles that went into P1, $N^{P1}_{\beta,tot}$, is the sum of the detected , $N^{P1}_{\beta,detected}$, and the added correction, corr. Assuming no angular correlation at all, the expectation is

$$N^{p1}_{\beta,tot} = N^{U1,U3,U6}_{\alpha} \times \frac{\Omega_{P1}}{4\pi}, \tag{4}$$

where $N^{U1,U3,U6}_{\alpha}$ is the total number of α-particles in U1, U3, and U6, and $\frac{\Omega_{p1}}{4\pi}$ is the fractional solid angle that P1 occupies. The solid angle that detector P1 occupies is given by the formula (Mathar 2014):

$$\Omega_{P1} = 4 \arccos \sqrt{\frac{1 + a^2/(4d^2) + b^2/(4d^2)}{(1 + a^2/(4d^2))(1 + b^2/(4d^2))}}, \tag{5}$$

where a is the width of the detector, b is the height, and d is the distance from target to center. The distances can be found from the plot in Figure 18 in the Appendix. The detectors are 50 x 50 mm. Also, for the expected number for U5, still assuming no correlation, should have another correction since the detector was blocked by the aluminum stand that held the target, lowering the number of particles that can get to U5. This effect is clearly seen in Figure 15 that shows a plot of the counts in the front strips against counts in the back strips. The diagonal (about 25-30 "tiles") have been blocked by the sample holder, and also a strip has not been active. A rough estimate of the reduction in solid angle is modelled as though the detector has been reduced with a strip in each dimension, which from formula 5 gives a reduction of 9 %.

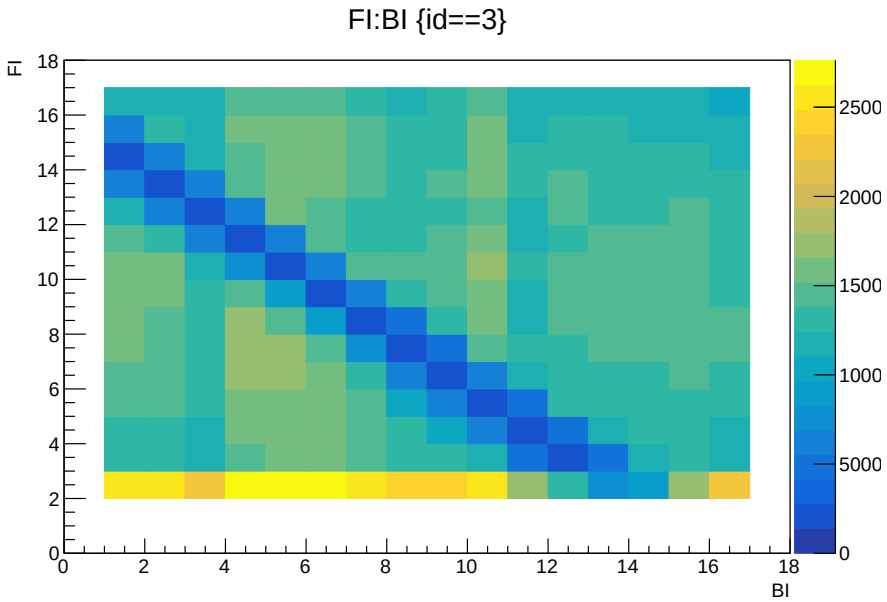

Figure 15: Strip-hit of U5. It is seen that strip 1 is missing and also that the diagonal has been blocked by the sample holder.

A final correction needed to be considered is the β detection efficiency of the detectors. By looking at the detection spectra and the ones appearing in reference (Berger et al. 1969), it is concluded that the efficiency is at least around 95 %. This value is used.

Estimating corrections: First approach

Having calculated the expected values, two approaches to compensate for the cutoffs are presented. The first approach is motivated by the fact that the spectra in Figures 12, 13 look as if they are roughly constant from the cutoff out to around energies of 400 keV where they begin to fall off for larger energies. Assuming that the number of counts is roughly constant below 400 KeV, the correction amounts to adding a rectangle of counts where the cutoff occurs. The number of counts in the rectangle should be in accordance with the average number of counts of the "constant" zone in the spectra. In the case of Figure 14, the behavior is a bit different, but the correction here is still to just assume that the counts would be constant from the cutoff down to zero.

In table 4 are seen some of the useful measurements and calculated values. The column with estimated *est. cutoff counts* needs some explanation. The numbers have been calculated by finding the average counts per keV for the "constant" part of the spectrum. Thus the constant part of P1 was from 50 to 550 keV, and for P3 from 50 to 500 keV. U5 is a bit tricky with this method, since it does not have the same form as the PADs. Depending on how big an interval one averages over, the counts per keV should then be multiplied with 45 keV, where the cutoff is. A lower limit at 13 counts has been found, and the upper limit has been estimated to $0.9982 \cdot 45 \approx 45$. The estimated corrections, i.e. extra counts added to each detector, are for P1 8.6 % of the initial counts, 9 % for P3, and between 2.3 % and 8.1 % for U5. For U5 the upper limit is chosen. Recall, that these percentages were made from the spectra in Figures 12, 13, and 14 which had data for *all* detected β-particles in each detector. The real task is to estimate corrections for the 9 cases in Table 3 that each have spectra with less statistics and less clear shapes. Thus, the correction percentages are taken as unique to each detector and used for the appropriate cases.

Using this approach, the new counts along with expected counts are shown Table 5. It is not obvious if there is any tendency of correlation in the numbers.

Preliminary calculations - expected values and corrections

Detector	d (mm)	$\Omega/4\pi$	est. correction
P1	45.72	0.0739	0.818 counts/keV · 50 keV ≈ 41 counts
P3	44.72	0.0765	0.7844 counts/keV · 50 keV ≈ 39 counts
U5	37.50	0.0996	13-45 counts

Table 4: Preliminary calculations associated with the detectors. These will be used to estimate the total number of measured and expected β-particles.

Distribution of β-particles - approach 1

α in DSSD (id)	β in P1	β in P3	β in U5
U1 (0)	193(14)/178	186(14)/184	207(14)/219
U3 (1)	165(13)/139	137(12)/144	178(13)/170
U6 (4)	161(13)/141	147(12)/145	217(15)/172

Table 5: The table shows measured/expected β-counts. The measured β-particles are with the "constant"-assumption correction added. Also, the expected number of β-particles is under the assumption of no angular correlation between α- and β-particles. Uncertainties are given in parenthesis, and are from assuming a Poisson distribution. The uncertainties on the expected values are assumed negligible.

Estimating corrections: Second approach

The second approach to estimating the corrections on the β-particle counts is motivated by the fact that the spectra in Figures 12 and 13 both seem to behave as typical β spectra (see Equation 6 below) that fall off as the energy approaches zero but with some noise at low energies that blur this fall off. For instance, in Figure 12 there is a local minimum at around 180 keV which could be where the natural fall off the β-spectrum meets the noise. To estimate the cutoff counts, a bigger cutoff is made manually to get rid of what could be noise. Following this a functional fit of the data is made. The fitting function describing a β-decay energy distribution is (Dunlap 2003, p. 113):

$$N(T_e) = \xi(T_e^2 + 2T_e \cdot m_e c^2)^{1/2}(Q - T_e)^2(T_e + m_e c^2), \tag{6}$$

where ξ is some constant, a fit parameter, and Q is the Q-value of the reaction, set to 0.9 MeV in this case, T_e is the electronic energy, and N_e is the number of particles. An example of such a fit is seen in Figure 16. The cutoff is at 210 keV and although the fit is not very good, it is only the ratio of the area under the graph before and after the cutoff that matters. This gives a ratio from which the counts beneath the cutoff can be found. Doing this for all 9 cases yields the data seen in Table 6. The estimated values are the same as for approach 1. To estimate if there is any correlation, a χ^2-independence test is used. Both correctional approaches are tested. The formula for the ξ^2-text size is:

$$\chi^2 = \sum_{i=1}^{9} \frac{(x_i - \bar{\mu_i})^2}{\sigma_i^2}, \tag{7}$$

where x_i is the number of detected β-particles in one detector, P1 say, given an α in one detector, U1 say, with correction added, $\bar{\mu}_i$ is the expected value associated with x_i, and σ_i is the uncertainty of x_i. The test size is calculated for Tables 5 and 6. Note that the uncertainty on the measured data is just under the assumption that they are Poisson distributed, but since the counts are small they can be taken as normally distributed which justifies the use of Equation 7. The degrees of freedom are 9.

β-spectrum and fit - example

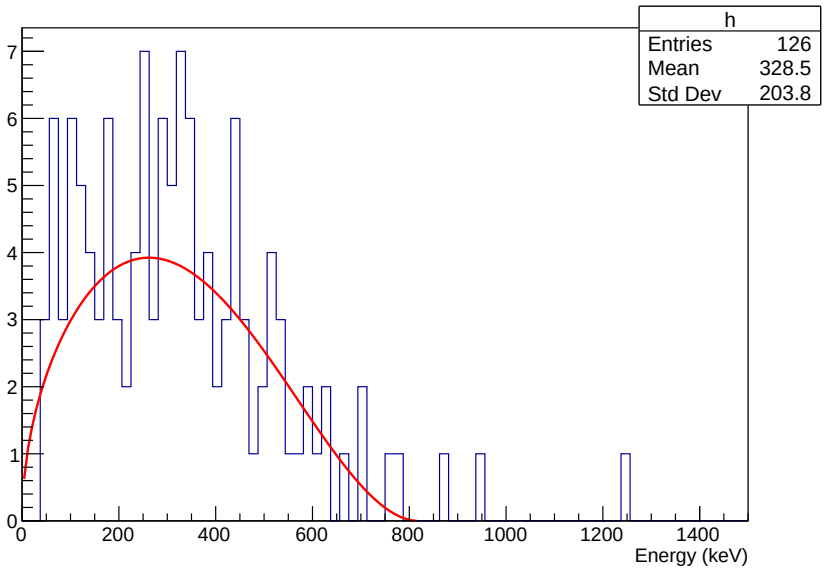

Figure 16: An example of a β-spectrum with a fit. The fit is not very good, but since only the ratio of the counts below and above cutoff, at 210 keV here, is needed, it is still useful. The spectrum is of β-particles in P3 given an α-particle in U3.

Distribution of β-particles - approach 2

α in DSSD (id)	β in P1	β in P3	β in U5
U1	183(14)/178	182(13)/184	204(14)/219
U3	156(12)/139	126(11)/144	181(13)/170
U6	148(12)/141	137(12)/145	219(15)/172

Table 6: The table shows the measured β-particles with a correction determined from fit. Expected values is if one assumes no angular correlation between α- and β-particles and are the same as in Table 5.

For the data in Table 5 the test size is $\chi^2 = 18.0167$ and for 9 degrees of freedom this yields a p-value of 0.035. For the second approach the test size is $\chi^2 = 17.3$ which for 9 degrees of freedom has a p-value of 0.044. These p-values are slightly significant which means that the null hypothesis that there is no angular correlation between α and β cannot be abandoned, and the data thus shows a small angular correlation. The first approach shows more significance than the second approach. However, one should note that uncertainties for the expected values have been neglected. From the findings in section 4 the

uncertainty in target position is evident and this will propagate as uncertainty in the calculation of the solid angle. There is also an uncertainty in the number of detected α-particles from which the expected number of β-particles is calculated. Including uncertainties like these will diminish the χ^2 test size and make the results less significant. These calculations are not carried out in this project, but especially approach 2, which is belied to be the more physically correct of the two, should then show very little to no correlation at all. This result seems sensible since it is hard to imagine that the β- and α-particles should show strong correlation because they are from roughly independent reactions.

As a back of the envelope consideration, Figure 17 is a rough sketch of the important angles in order to calculate the angular correlation between the antineutrino and β-particle. In this project, the energies and relative angle between α-^{12}C are found which, if the experiment had been sensitive towards recoil and less dependent on beam spread and position, could give the momentum of the recoiling $^{16}O^*$. The relative angle between α-β, v_2, could have been calculated if the PADs had a spatial resolution. However, the PADs are unsegmented and only a test for large scale angular correlation could be made in this project. Assuming again that the $^{16}O^*$-momentum was known, the β-energy in combination with $v_3 = \pi - v_1 - v_2$ could give the β-momentum and finally its angular correlation with the antineutrino. These considerations can be made much less hand-wavy, but the point with this discussion is merely to show that the lack of sensitivity in $^{16}O^*$-recoil and the lack of spatial resolution in the PADs are a limiting factor in terms of what can be pulled out from this data set.

Sketch of relevant angles

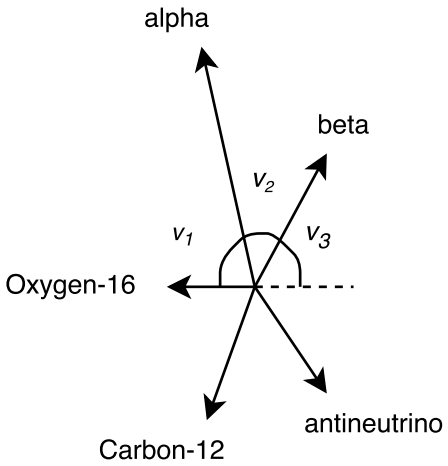

Figure 17: A rough sketch of the relevant angles, momentum vectors not drawn to scale. Knowledge of v_1, v_2 and v_3 could yield the angular correlation between the β and antineutrino.

7 Conclusion

This project has investigated data from the ISOLDE-experiment IS605 from May 2016. DSSDs U1, U3, and U6 from the experiment were thin enough to separate the α- and β-particles in the energy spectrum. Detectors U1 and U6 are opposite each other and the angular distribution of α- and ^{12}C-pairs have been retrieved. This has been compared to a Monte Carlo simulation of the relevant reaction. The simulated angular distributions show great dependence on beam width (beam of ^{16}N hitting target) and position. The point (1.5, 0, -2.7) has been used for the beam position in the simulation and provides good discrepancy between experimental and simulated data. Any small discrepancies could be because of the uncertainty in what the actual beam position was in the experiment. The simulated data does not seem to show much dependence on whether a recoil of $^{16}O^*$ is accounted for or not. A smaller pixel size of the detectors would be needed to observe the effect. Angular correlations between α- and β-particles have been studied at large scales. β energy spectra in the PADs have first been characterized. PADs P6 and P4 have spectra that are disturbed by outer factors and were therefore not used. Given an α-particle in one of the DSSDs U1, U3 or U6, the associated β-particle detection in either P1, P3 or the DSSD U5 has been noted. The angular correlation between α- and β-particles has been estimated by introducing a correction to the low energy counts in the β-spectra. Two correctional approaches have been attempted. A χ^2-independence test for correlation yields p-values of 0.035 and 0.044 for approach 1 and 2, respectively. The p-values are estimated to be higher than this because of negligence of uncertainties in the expected

values. All in all, little or no correlation is found. This is especially the case when using correctional approach 2, that is believed to be the more physically sound of the two. Given the lack of sensitivity towards recoil of ^{16}O and lack of spatial resolution of the PADs, angular correlation between ^{16}O and β-particles will be difficult to investigate with the given data.

References

Berger, M. et al. (1969). 'Response of silicon detectors to monoenergetic electrons with energies between 0.15 and 5.0 MeV'. In: *Nuclear Instruments and Methods* 69.2, pp. 181–193.

Dunlap, R. A. (2003). *An introduction to the physics of nuclei and particles*. Thomson/Brooks-Cole.

Fynbo, H., O. S. Kirseboom, and O. Tengblad (2017). 'ISOLDE decay station for decay studies of interest in astrophysics and exotic nuclei'. In: *Journal of Physics G: Nuclear and Particle Physics* 44.4, p. 044005.

Hong, R., M. G. Sternberg, and A. Garcia (2017). 'Helicity and nuclear β decay correlations'. In: *American Journal of Physics* 85.1, pp. 45–53.

Mathar, R. J. (2014). 'Solid angle of a rectangular plate'. In: *Max-Planck Institute of Astronomy, Königstuhl* 17, p. 69117.

8 Appendix

β-distributions, given both α and ^{12}C

The Table 7 shows the distributions of β-particles given *both* an α- and a ^{12}C-particle, as opposed to Table 2. As discussed above, for α and ^{12}C coincidences, it is a good approximation to take two opposite detectors and demand multiplicity equal to two. So for each of the points in Figure 4, it is recorded if there was also detected a β-particle in one of the PADs. The statistics are seen in Table Figure 7. Again P6 seems to be overrepresented when one takes into account its thickness. On a positive note, the percentages for the different PADs are relatively unchanged between the two tables in 2 and 7, which is expected since the physics should be the same whether ^{12}C is detected or not.

β-distributions, given α and ^{12}C

α in DSSD (id)	#α-C12	#β, %	P1 %	P3 %	P4 %	P6 %	U5 %
U1 (0)	1713	1043, 60.9	10.9	10.1	4.3	61.6	13.1
U3 (1)	1335	867, 64.9	12.5	9.7	5.7	59.2	13.0
U6 (4)	1386	896, 64.6	12.1	10.6	4.5	56.7	16.2

Table 7: Table showing number and distributions for α-^{12}C-β-incidences. For each α-^{12}C-detection there can be a β-detection, and the column #β gives the number of times a β-particle was also detected. For each pad there is a column specifying the percentages of β's that were detected here. E.g., 1713 α-^{12}C-events were recorded in U1, 60.9 % of these, 1043, had an associated β-detection in a pad, and 10.9 % of these were detected in P1.

Experimental set up - distances

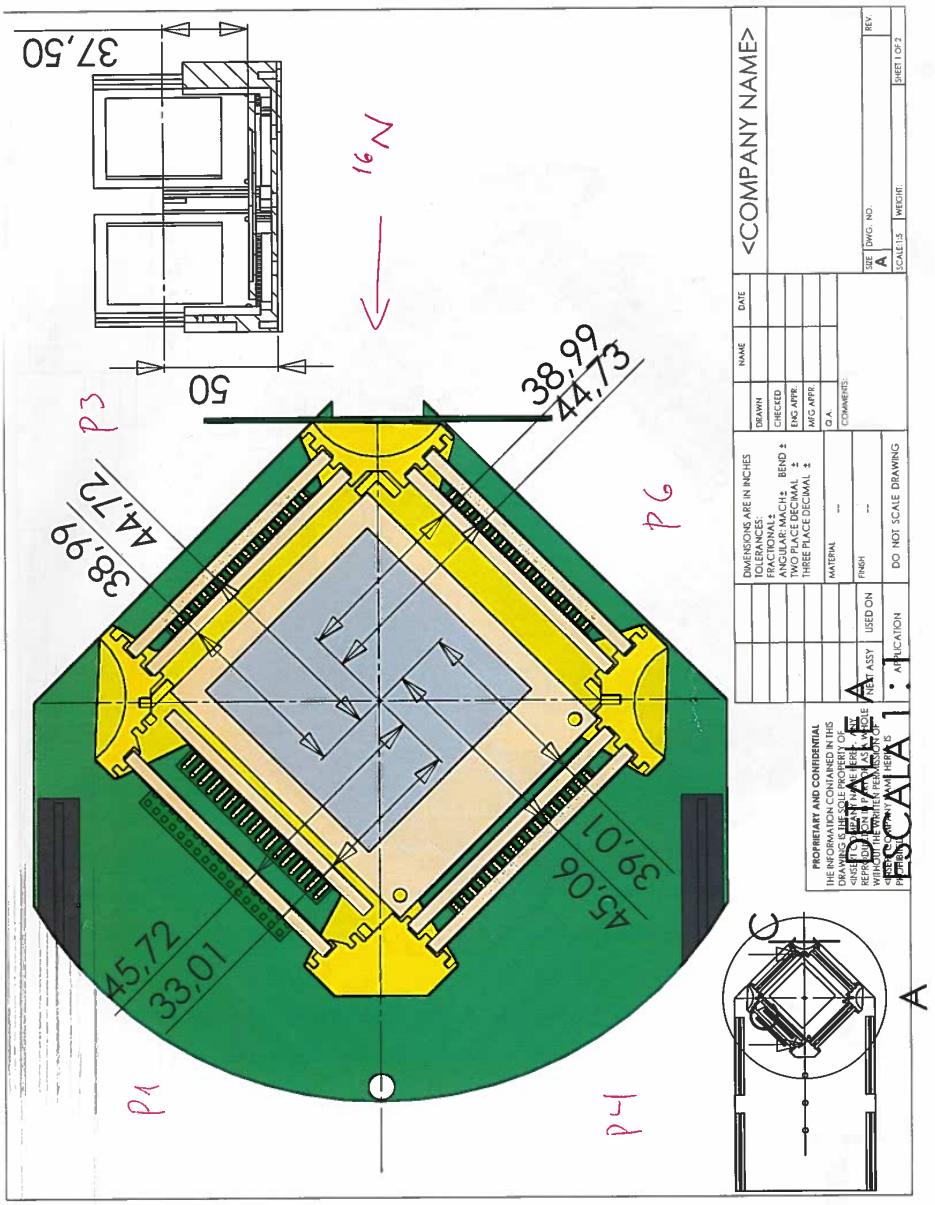

Figure 18: The experimental set up seen from above. This paper gives the distances between the PADs and the target, assuming the target is in the origin. These distances are used in the calculation of expected values with regards to β-particles distribution in the PADs.